Plumes and waves in two-dimensional turbulent thermal convection

Alain P. Vincent

*Département de Physique, Université de Montréal C.P. 6128, Succursale A, Montréal, Québec, Canada H3C 3J7
and CERCA, 5160 Boulevard Décarie, Bureau 400, Montréal, Québec, Canada H3X 2H9*

David A. Yuen

*Minnesota Supercomputer Institute and Department of Geology and Geophysics, University of Minnesota,
Minneapolis, Minnesota 55415-1227*

We have conducted a high-resolution, two-dimensional direct numerical simulation of Rayleigh-Bénard convection with stress-free and periodic boundary conditions at a Rayleigh (Ra) number of 10^8 and Prandtl (Pr) number of unity. An aspect-ratio three box has been considered. A single cell has been used as the initial condition. First, the flow develops into time-dependent convection with a strong asymmetry and highly convoluted thermal plumes delineating a large-scale circulation. Smaller thermal plumes detach from the boundary layer and extend over the entire cell, creating a local inversion of the temperature gradient adjacent to the boundary layers. Then the conditions leading to the formation of internal waves are fulfilled, as the local Richardson number decreases sufficiently small to cross the linear threshold of Ri=0.25. Together with the strong shear, convective rolls with a Kelvin-Helmholtz wavelike character are produced. The secondary boundary layer itself becomes unstable and produces smaller plumes. At later times, the large-scale circulation is destroyed and the internal waves disappear. A Reynolds number, based on the global scale, of Re=500, is attained at this stage. Only isolated thermal plumes and vortices are present. Thus, internal waves can be generated at finite Prandtl number fluids for sufficiently high Ra in the presence of a large-scale circulation. Spectral analysis reveals that the kinetic energy decays with a logarithmic slope of -3, while the logarithmic slope of the thermal variance has a value of around $-\frac{5}{3}$. [S1063-651X(99)05709-8]

PACS number(s): 05.60.−k

I. INTRODUCTION

Turbulent convection has been studied experimentally for many years, but much impetus has been provided by the concept of ''hard-turbulent'' convection in the last decade [1,2]. Ra as high as 10^{14} has been reached in the laboratory [3]. Experiments have been conducted in low Prandtl fluids of helium gas [1] and in water [3]. One of the primary signatures of ''hard-turbulent'' convection has been suggested to be the prevalence of disconnected plumes, which are unable to reach the opposite thermal boundary layer. Such a scenario, together with a strong ''wind'' associated with a large-scale circulation, is well suited for creating just atop the thermal boundary layers, a local inversion in the temperature gradient. Thus, this region becomes thermally stably stratified and internal waves can be generated there, in the presence of a sufficiently strong shear flow. Hence, the characteristic frequency recorded by Castaing *et al.* [2], Wu *et al.* [4], and Vincent *et al.* [5] is the well-known Brunt-Väisälä frequency. Numerous experimental and theoretical studies have been carried out since that time on the shear interaction near the thermal boundaries [6–9].

The other fundamental issue of convective turbulence is whether the scaling of the Nusselt number (Nu) with Ra goes as Nu≈Ra$^{2/7}$. Spectral characteristics of ''hard-turbulent'' convection show that there exist logarithmic slopes as a function of the shell averaged wave number. For the kinetic energy spectrum, a value of around $-\frac{11}{5}$ has been found for the logarithmic slope, while for the variance of the thermal fluctuations a value of $-\frac{7}{5}$ has been inferred [10,11]. Such a scaling has been proposed on physical grounds by Castaing *et al.* [2] and is due to a thermally stratified mechanism [12,13], but inconsistencies with the Boussinesq, incompressible approximation have also been noted [8,14].

Compared to laboratory experiments, numerical studies of ''hard-turbulent'' convection have been few and far between, because of the inherent technical differences in the computational infrastructure of many institutions. A few numerical studies have been conducted for three-dimensions either with stress-free [15,16] or with rigid boundaries [17,18]. In spite of the simplification of the physics, two-dimensional simulations represent logically a first step to study this problem, as one can carry out the computation and the visualization much easier than for the much more cumbersome three-dimensional (3D) simulations. Werne and co-workers [19,20] have studied from 2D simulations the soft to ''hard-tubulent'' convection and plume dynamics [21], but these studies were restricted to Ra less than 5×10^7. In this study we will use a spectral method with a high-resolution grid to study convection of Ra ranging from 10^7 to 10^8, as we are interested in the development of waves and subsequent bifurcations in the plume dynamics.

We emphasize here that direct numerical simulations (DNS) are needed to unveil new phenomena, especially those concerned with the formation of secondary and tertiary plumes and waves and their nonlinear interaction with the boundary layers. The purpose of this work is to obtain a high-quality DNS solution of a complicated flow before we will attempt to simulate this with the large-eddy simulation (LES) approximation (e.g., Ref. [22]).

II. NUMERICAL ALGORITHM

The dimensionless equations describing finite Prandtl number convection are in the Boussinesq approximation

$$\nabla \cdot \mathbf{V} = 0, \tag{1}$$

$$\frac{\partial \mathbf{V}}{\partial t} = \mathrm{Pr}\Delta \mathbf{V} + \mathbf{P}(\mathbf{V} \mathbf{x} \boldsymbol{\omega} + \mathrm{Pr}\, T \mathbf{e_z}), \tag{2}$$

$$\frac{\partial T}{\partial t} + \nabla \cdot (\mathbf{V}T) = \Delta T + \mathrm{Ra}\, V_z \mathbf{e_z}, \tag{3}$$

where t is the dimensionless time based on thermal diffusion, T is the temperature deviation from the linear profile, ω is the vorticity, and e_z is the vertical unit vector directed from the top to the bottom of the fluid layer. Ra is the thermal Rayleigh number for pure based-heating and Pr is the Prandtl number. We have taken a Pr number of unity.

The scale units are the thickness of the layer, the thermal diffusive time and the temperature difference between top and bottom divided by the Rayleigh number. The thermal diffusive time is the proper scale for large Prandtl thermal turbulence. For very small Pr, the viscous-diffusive time would be a more suitable choice.

The numerical method used here is a spectral method, which is based on the sine-cosine functions that are naturally ensuring the top and bottom free-slip boundary conditions for the velocity, vertical fixed temperature gradient and horizontal periodicity. Such methods have been largely in use for thermal convection for finite Pr (e.g., Ref. [15]). The time marching is a mixed leap-frog–Crank-Nicholson two-step scheme. We have used a modified version of a two-dimensional code written originally for double diffusive convection [23]. $\mathbf{P}$ is the usual divergence-free spectral projector $[P_{ij} = (\delta_{ij} - k_i k_j/k^2)]$, with k being the wave number. This is exactly equivalent to carrying out a two-step pressure correction scheme for the momentum equation.

Since the thickness of the boundary layers varies like $\delta \approx \mathrm{Ra}^{1/3}$ and one can expect that the plumes are detached parts of the boundary layers, the minimum number of (equally spaced) grid points varies such as $N \approx \mathrm{Ra}^{2/3}$. For very large Rayleigh numbers and outside the boundary layers, the assumption of thermal and velocity homogeneities is reasonable. The aspect ratio is 3 and the initial condition is a large scale flow, i.e., a single cell. The grid is equally spaced with spectral accuracy and the number of grid points is $N_z = 256$ and $N_x = 768$ for $\mathrm{Ra} = 10^8$. Together with the temperature equation, we computed the evolution of a Lagrangian tracer distribution

$$\frac{\partial C}{\partial t} + \nabla \cdot (\mathbf{V}C) = 0. \tag{4}$$

where C is the tracer concentration. We started all runs with a linear profile as the conducting temperature profile. The local (gradient) Richardson number (e.g., Ref. [24])

$$\mathrm{Ri} = \frac{1}{T_0} \frac{\partial \delta T}{\partial z} \left(\frac{\partial V_x}{\partial z} \right)^{-2} \tag{5}$$
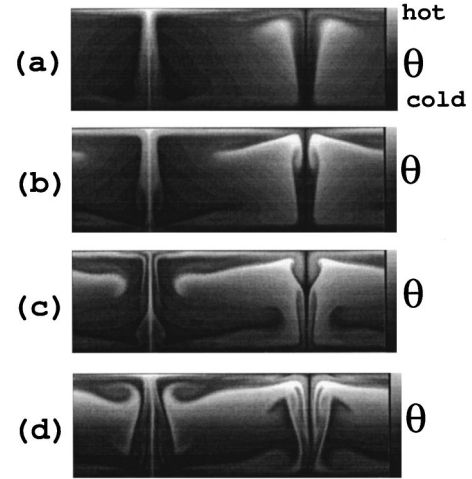

FIG. 1. Convective temperature field. Sizes of the box are $L_x = 3$, $L_z = 1$. The Rayleigh number is $\mathrm{Ra} = 10^8$ and the Prandtl number is $\mathrm{Pr} = 1$. The numerical resolution is $N_x = 768$, $N_z = 256$ grid points. Temperature history between thermal diffusive time $t = 3 \times 10^{-3}$ TDT (thermal diffusive time) (a) and $t = 6 \times 10^{-3}$ TDT (d). Time interval between two consecutive figures is $t = 10^{-3}$ TDT. Initial conditions are two large counterrotating rolls. (a) $t = 3 \times 10^{-3}$ TDT. Small plume appears near the top and thus an internal thermal boundary layer is developed. Those plumes are bent by the very strong horizontal velocity creating a local inversion of the temperature gradient and thus an internal thermal boundary layer. This creates an ideal condition for internal waves to develop. (b) $t = 4 \times 10^{-3}$ TDT. The wave breaks at the extremity of the new thermal boundary layer (see the arrow). (c) $t = 5 \times 10^{-3}$ TDT. (d) $t = 6 \times 10^{-3}$ TDT. Originating from the major ascending plume (right) and breaking near the other major descending plume (left), the new thermal boundary layer extends now horizontally over the whole cell. Later on, secondary thermal plumes will be created from this secondary internal horizontal thermal boundary layer.

is the ratio between the square of the buoyancy and turnover frequencies

$$\mathrm{Ri} = N^2 \left(\frac{\partial V_z}{\partial z} \right)^{-2}, \tag{6}$$

where N is the buoyancy (Brunt-Väisälä) frequency written in terms of the temperature and viscous-diffusive time units

$$N^2 = \frac{1}{T_0} \frac{\partial \delta T}{\partial z}. \tag{7}$$

Here δT is the convective thermal deviation from the linear profile. If the local Richardson number decays below $\mathrm{Ri} = 0.25$, the layer is linearly unstable to internal waves (e.g., Ref. [25]). The minima for Ri correspond to highest inverse temperature gradients and the almost horizontal inverse layers thus gravity can play the role of a restoring force. Another dynamical output in finite Pr convective flow is the Reynolds number Re, which measures the vigor of inertial forces.

III. RESULTS

We have initialized the solutions with two cells in an aspect-ratio three box. Steady states were obtained for Ra
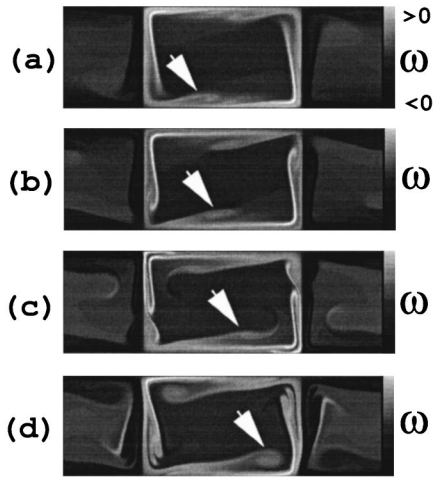
FIG. 2. Transverse vorticity ω corresponding to Figs. 1(a)–1(d).

ranging between 10^5 and 10^7 by integrating up to 20 000 time steps (1 time step$=10^{-6}$ TDT). Other types of initial conditions may induce chaotic time-dependence even for Ra numbers as low as 3×10^5, as shown in the work on infinite Prandtl number convection [26]. For these initial conditions, the first interesting time-dependent activity was observed at 10^8 and we will focus our attention on this high Rayleigh number because of the interesting dynamical features developed, such as the waves. Such a high Rayleigh number of 10^8 has not been investigated before in two-dimensional finite-Prandtl number convection.

A. Incipient stage

Convection at high Rayleigh number is characterized in the ''hard-turbulent'' regime by filaments and patches of thermal anomalies with opposite signs [2]. In these circumstances, the juxtaposition of hot and cold thermal anomalies becomes the rule rather than the exception. In Fig. 1 we plot
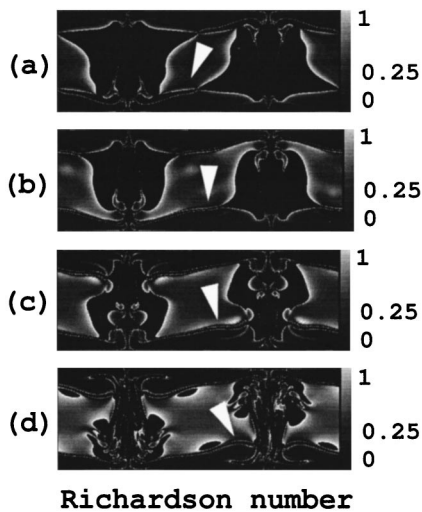

FIG. 3. Local Richardson number corresponding to Figs. 1(a)–1(d). Color scale is for Ri<0.25. Black denotes values above Ri >0.25. The Ri$=\frac{1}{4}$ values for the Richardson number are located mainly at the strong temperature gradients but internal waves can only be produced at the instant where the corresponding layers are almost horizontal.
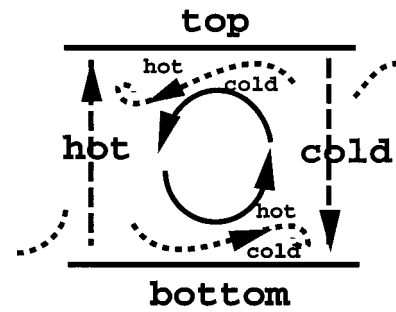

FIG. 4. Schematic of flow fields displayed in Figs. 1–3. The vertical flows have a tendency to split into secondary tributaries, similar to a river delta. We observe here the double-decker nature of the horizontal boundary layers, consisting of a juxtaposition of hot and cold anomalies overlying one another. Internal waves are developed along the interface of this double-decker boundary layer.

the snapshots of convected thermal anomaly θ, which is defined to be the total temperature T minus the conductive temperature profile $T_c(z)$. These panels have been taken from the early stages in the flow development, following the initial transient. Figure 1 shows the development of the cold and hot plumes diving into the opposite bottom and top boundary layers and branching in the process. This type of strong boundary-layer interaction produces secondary hot and cold flows to develop, giving rise to a whirling interior flow. The schematic of this type of flow is sketched in Fig. 4. The vertical flows have a tendency to split into secondary tributaries, similar to a river delta. We see here the double-decker nature of the horizontal boundary layers, consisting of a juxtaposition of hot and cold anomalies overlying one another. This condition is favorable to the production of internal waves, which are observed to develop along the interface of this double-decker boundary layer.

Figure 2 shows the corresponding temporal development of the vorticity ω. The light and dark colors denote respectively the positive and negative values of the vorticity. The
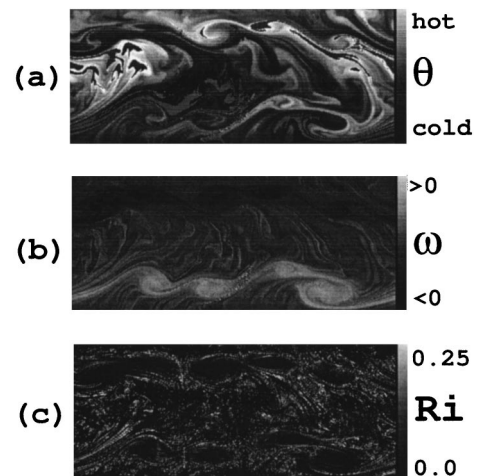

FIG. 5. Subsequent evolution of the shear layer at time t $=0.3 \ 10^{-2}$ TDT after the shear has been initiated near the boundary layers. (a) Temperature fluctuation θ. (b) Transverse vorticity ω. (c) Local Richardson number Ri. Only values ranging for Ri <0.25 are shown. Otherwise, black color for higher values.
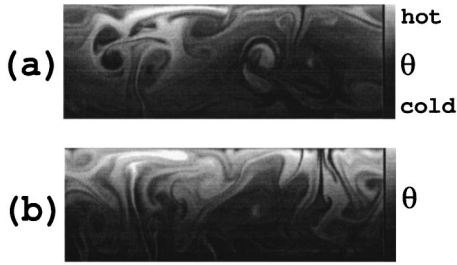
FIG. 6. Two subsequent snapshots of the convected thermal anomaly θ. (a) Time is $t=0.9 \; 10^{-2}$ TDT. (b) Time is $t=1.5 \; 10^{-2}$ TDT.

wave nature is more clearly delineated by the vorticity signature. Its development at the bottom boundary layer is illustrated by the arrow in the figure. The Richardson number Ri serves as a linear criterion for the development of secondary shear instabilities in stratified flows (e.g., Ref. [25]). For Ri less than $\frac{1}{4}$, shear instabilities can develop according to linear theory [24]. In Fig. 3 we have plotted the spatial distribution of the local Ri associated with the frames shown in Fig. 1. We have thresholded the values of Ri to black for Ri above 1. The white arrows in Fig. 3 point out the boundary for Ri=0.25, which coincides with the waves shown in Fig. 2. Sharp fronts with Ri<0.25 are found at narrow zones with sharp gradients in the convected temperature field. In these zones there is a strong tendency for shear instabilities to develop and to produce wavelike features. In terms of being a valuable diagnostic tool for detecting the onset of wavelike structures in thermal convection, the sharp boundaries of the Ri distribution yield the sharpest and clearest signature of all of the fields displayed up to now. Figure 4 shows a schematic of this type of wavelike flow.

In order to validate the idea of the Richardson number mapping coherently with the other dynamical quantities, we have conducted the following experiment. We started a simulation with, as initial conditions, a statistically stationary convective flow at Rayleigh number Ra=10^8. At time t=0, we also input a strong shear near the top and bottom boundary layers. Then we have run the simulation with no further perturbation. After 30 000 time steps, corresponding to thermal diffusive time t=0.03 TDT units, we obtained, as expected, a Kelvin-Helmholtz wavelike pattern at the boundaries. The wave patterns are displayed clearly in Fig. 5 for the temperature deviation [Fig. 5(a)], the vorticity [Fig. 5(b)], and the values of the Richardson number smaller than Ri=0.25 [Fig. 5(c)].

B. Subsequent development

The flow fields at Ra=10^8 become evermore complex with time. In Fig. 6 we show two subsequent snapshots of the convected thermal anomaly $\theta(z)=T-\langle T\rangle(z)$. We ob-
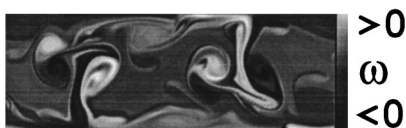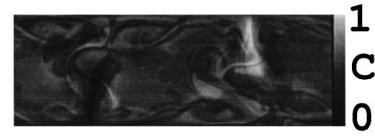

FIG. 8. Tracer concentration C corresponding to Fig. 6(a). Concentration gradients are located where the high vorticity gradients are. In two-dimensional turbulence, the vorticity variance is a conserved quantity.

serve that many thermal inversions begin to appear and the plumes do not reach the opposite side, as characteristic of ''hard-turbulent'' convection. The last vestiges of cellular structure are destroyed in Fig. 6(b), as small-scale features dominate from this point on. The Reynolds number of the convective flow based on the integral scale of $l_{oz}\approx0.25$ is Re$\approx$500, while the Reynolds number based on the Taylor microscale of $\lambda\approx0.1$ is Re$_\lambda\approx$200. In Fig. 7 we show the transverse component of the vorticity ω_y, which reveals the complicated nature of the vortex dynamics of the plumes as for instance the two pairs of vortices (dipoles). The concentration field is another signature which can reveal the cumulative history of the dynamics as in the mixing of a passive scalar. In Fig. 8 we plot the cumulative history of the mixing of the concentration. This panel represents the superposition of the many images and gives an idea of the overall dynamics of the passive scalar field. Figure 8 shows a threshold image of the mixing and emphasizes the coherent features of the plumes.

The spatial distribution of the local Nusselt number yields valuable information of the convective flux locally. This quantity Nu(x,z,t) can be evaluated at each time step by evaluating a local integral about the grid point. In Fig. 9 we display the local Nu field for the time step corresponding to Fig. 6(a). There is a maximum peak heat transfer in the heart of the plumes from the local advection. The vast disparity of the local Nu field in ''hard-turbulent'' convection has also been pointed out by Grossmann and Lohse [9] using the Fourier-Weierstrass expansion technique. The local Ri distribution for this same panel is shown in Fig. 10. We can observe that the zones of shear instabilities have become extremely localized and widespread, similar to the fractured patterns in solids [27]. Again, it is evident that the sharpness of the Ri signal in detecting shear instabilities is clearly superior to the other signatures.

IV. STATISTICAL ANALYSIS

In this section we will focus on the statistical treatment of the flow data for the various signatures. First, we present in Fig. 11 the shell averaged spectrum of the kinetic energy

FIG. 7. Transverse vorticity ω corresponding to Fig. 6(a). The plumes consist of two counter-rotating vortices.
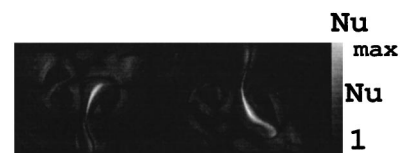

FIG. 9. Local Nusselt number Nu corresponding to Fig. 6(a). The Nusselt number is maximal in the plumes, where the convective heat flux is the greatest.
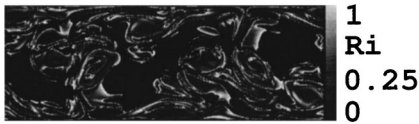
FIG. 10. Local Richardson number Ri corresponding to Fig. 6(a). Minima for the Richardson number are located mainly where the temperature gradients are but internal waves can be created only when and where the corresponding layers are almost horizontal.

$KE(k)$, which has been obtained by integrating over the modulus of k and over the last 100 000 time steps. The grid resolution is demonstrated to be quite adequate, as revealed by the sharp drop in the spectral content. Plotted above the calculated spectrum is a fiducial line with a logarithmic slope of -3. The dissipative range is seen to lie beyond k greater than 30. A comparison of this with the -3 slope shows that the flow has intrinsically 2D turbulent properties as shown by Refs. [28–30]. It also demonstrates the property of a direct cascade of the enstrophy at large k (e.g., Refs. [31, 28].

The shell averaged spectrum of the variance of the convected thermal anomaly θ, averaged over time as in Fig. 11, is displayed in Fig. 12. We have plotted a fiducial curve with a logarithmic slope of $-\frac{5}{3}$ for visual comparison. A slope of $-\frac{5}{3}$ for the variance in ''hard-turbulent'' convection has been predicted theoretically by Lohse [32]. Our slope for the thermal variance comes close to the $-\frac{5}{3}$ value in the spectral region before the dissipative range, which begins somewhere for k greater than around 40. This slope indicates some sort of inverse cascade of the energy (e.g., Ref. [31]).

The frequency spectra of the variance should bear some relationship to the spatial spectra according to Taylor's hypothesis [33] and also Chilla *et al.* [34]. In Fig. 13 we plot the frequency spectrum of the thermal anomaly θ along with a fiducial line with a logarithmic slope of $-\frac{5}{3}$. The correlation between Figs. 12 and 13 is better for low values of k and ω.

In strongly time-dependent convection with finite Prandtl number the thermal anomalies should behave as passive sca-
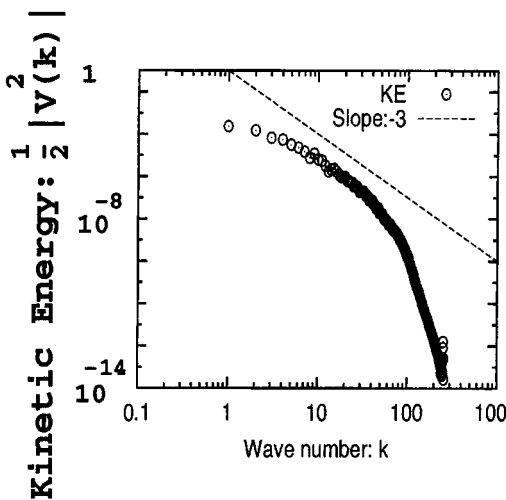

FIG. 11. Kinetic energy spectrum corresponding to the statistically steady state part of the run. The slope is k^{-3} as is the case in two-dimensional turbulence. E_x and E_z are the variance spectra for V_x and V_z.
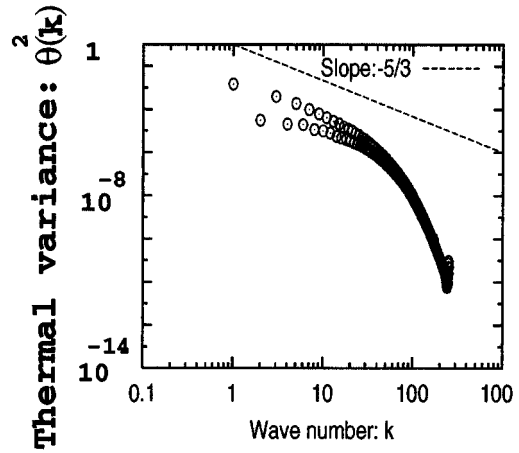

FIG. 12. Thermal variance spectrum corresponding to Fig. 1. The slope is $k^{-5/3}$. This indicates the presence of inverse cascade. The large-scale energy arises from the small thermal scales.

lars [35]. In Fig. 14 we plot the shell averaged spectrum of the passive scalar C and show by comparison with the fiducial line (slope of $-\frac{5}{3}$) that there is indeed a similarity of the spectrum of C to the spectrum of θ (Fig. 12). The probability distribution function (PDF) of C is shown in Fig. 15. An exponential fall-off is clearly evident from inspection of the figure. This exponential decay in the PDF agrees with the theoretical prediction of the PDF in high Rayleigh number convection for finite Prandtl number fluids by Yakhot [35].

V. CONCLUDING REMARKS

We have conducted a high-resolution numerical investigation of high Rayleigh number convection for Ra$=10^8$ and a Prandtl number of 1. These simulations employing the spectral methods, reveal many fine features, such as the presence of waves, a local inversion of temperature next to the boundary layers, and double-decker boundary layers, which have not been observed before in previous 2D simulations for finite Prandtl number convection [19,20] conducted for Ra between 10^7 and 10^8. Our two-dimensional simulations show that it may not be possible to maintain a large-scale flow under these ''hard-turbulent'' situations, because of the
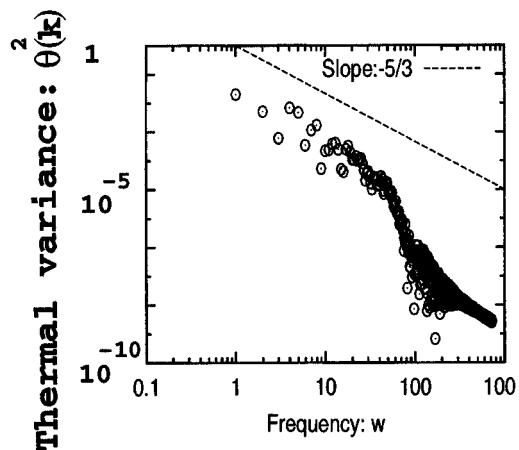

FIG. 13. Frequency spectrum of the time history of the thermal anomaly θ at a single point.
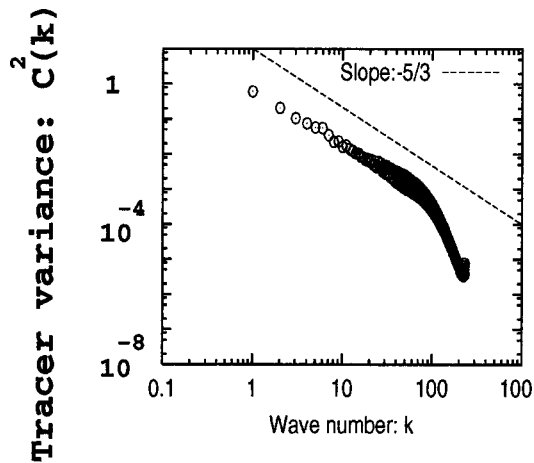
FIG. 14. Tracer variance spectrum corresponding to Fig. 8. The slope is $k^{-5/3}$. There is neither buoyancy nor dissipation acting on the tracer field. The tracer is focussed at where the entrosphy is large. The vortical part of the plumes (heads of the plumes) corresponds to vorticity and thus to inverse cascade of the kinetic energy.
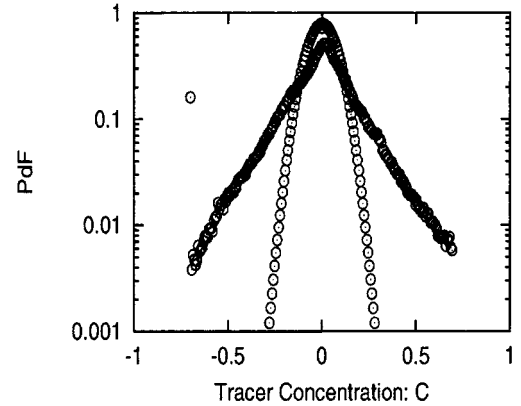

FIG. 15. Probability distribution function (PDF) of C corresponding to Fig. 14. Compared with a Gaussian peak with the same variance, the wings are exponential. This is related to intermittency in the turbulent flow.

ever-increasing time-dependent generation of smaller and smaller boundary layer instabilities. We have based these conclusions on a simulation, which has exceeded over 10^5 time steps.

We have observed the development of gravity waves in this high Ra convective flow and the generation of a secondary thermal boundary layer from a single elongated plume. Secondary plumes may be produced from this new internal boundary layer. The signature of the local Richardson number has revealed clearly the sites of these shear instabilities occurring within a buoyancy-driven flow. The distribution of the local Nusselt number also based shows that the most significant convective thermal transport induced by adjective straining are developed in the vertical plumes and they appear as discrete coherent structures embedded within the plumes. Similar signs of these localized features are also revealed by the vorticity and tracer distribution. Jetlike structures are found to develop and branch out within the vertical flows, as in a river approaching a delta.

Spectral analysis has shown that the thermal anomalies behave as a passive scalar from both the spectra of the thermal variance and the tracer field, which display a logarithmic slope of $-\frac{5}{3}$. On the other hand, the kinetic energy spectrum yields a logarithmic slope of -3, lending some support to the

flow behaving with two-dimensional turbulent characteristics.

With the current computational power (10 GF lops) and memory resources (up to 10 Gbytes), much higher Ra convection (up to 10^{14}) is very feasible in two-dimensions but much more difficult in 3D, because of both hardware and software issues dealing with storage of extremely large data sets and the attendant visualisation. To our mind, it is vitally important first to study in great detail the dynamics encountered at Ra$=10^8$, which represents a noticeable leap past the ''hard-turbulent'' boundary at around 4×10^7 [2,19,20]. In this study, we did not find any of the ''turbulent plumes'' predicted by Rieutord and Zahn [36] for stellar convection and seen in Brandenburg et $al.$ [37]. Perhaps they may occur at higher Rayleigh numbers. This is a subject for future study.

ACKNOWLEDGMENTS

[1] F. Heslot, B. Castaing, and A. Libchaber, Phys. Rev. **36**, 5870 (1987).

[2] B. Castaing, G. Gunaratne, F. Heslot, L. Kadanoff, A. Libchaber, S. Thomae, X. Zh. Wu, S. Zaleski, and G. Zanetti, J. Fluid Mech. **204**, 1 (1989).

[3] A. Belmonte, A. Tilgner, and A. Libchaber, Phys. Rev. E **50**, 269 (1994).

[4] X. Z. Wu, L. Kadanof, A. Libchaber, and M. Sano, Phys. Rev. Lett. **64**, 18 (1990); **64**, 2140 (1990).

[5] A. P. Vincent, U. Hansen, D. A. Yuen, A. V. Malevsky, and S. E. Langenberger, Phys. Fluids A **3**, 2222 (1991).

[6] T. H. Solomon and J. P. Gollub, Phys. Rev. Lett. **64**, 2382 (1990).

[7] T. H. Solomon and J. P. Gollub, Phys. Lett. A **43**, 6683 (1991).

[8] B. I. Shraiman and E. D. Siggia, Phys. Rev. A **42**, 6 (1990); **42**, 3650 (1990).

[9] S. Grossmann and D. Lohse, Phys. Lett. A **173**, 58 (1993).

[10] X. Z. Wu and A. Libchaber, Phys. Rev. A **45**, 842 (1992).

[11] X. Z. Wu, Ph.D. thesis, Department of Physics, The University of Chicago, 1991 (unpublished).

[12] R. Bolgiano, J. Geophys. Res. **64**, 12 (1959); **64**, 2226 (1959).

[13] A. M. Obukhov, Dokl. Akad. Nauk SSSR **125**, 6 (1959); **125**, 1246 (1959).

[14] E. D. Siggia, Annu. Rev. Fluid Mech. **26**, 137 (1994).

[15] S. Balachandar, M. R. Maxey, and L. Sirovich, J. Sci. Comput. **4**, 219 (1989).

[16] T. Cortese and S. Balachandar, Phys. Fluids **5**, 3226 (1993).

[17] R. M. Kerr, J. R. Herring, and A. Brandenburg, Chaos Solitons Fractals **5**, 2047 (1995).

[18] R. M. Kerr, J. Fluid Mech. **310**, 139 (1996).

[19] J. Werne, E. E. DeLuca, R. Rosner, and F. Cattaneo, Phys. Rev. Lett. **67**, 3519 (1991).

[20] J. Werne, Phys. Rev. E **49**, 5 (1994); **49**, 4072 (1994).

[21] C. Bizon, J. Werne, A. A. Predtechensky, K. Julien, W. D. McCormick, J. B. Swift, and H. L. Swinney, Chaos **7**, 107 (1997).

[22] M. Peric and J. H. Ferziger, *Computational Methods for Fluid Dynamics* (Springer, Berlin, 1996).

[23] A. Deane, URL http://sdcd.gsfc.nasa.gov/ESS/exchange/contrib/deane/ddcon2d.html, NASA/GSF, 1993.

[24] P. G. Drazin and W. H. Reid, *Hydrodynamic Stability* (Cambridge University Press, Cambridge, England, 1981).

[25] J. Pedlosky, *Geophysical Fluid Dynamics*, 2nd ed. (Springer Verlag, New York, 1987).

[26] A. P. Vincent and D. A. Yuen, Phys. Rev. A **38**, 1, 328 (1988).

[27] A. N. B. Poliakov and H. J. Hermann, Geophys. Res. Lett. **21**, 2143 (1994).

[28] M. Lesieur, *Turbulence in Fluids*, 3rd ed. (Kluwer Academic, Dordrecht, 1997).

[29] K. G. Oetzel and G. K. Vallis, Phys. Fluids **9**, 2991 (1997).

[30] J. C. McWilliams, J. Fluid Mech. **219**, 361 (1990).

[31] H. Tennekes and J. Lumley, *A First Course in Turbulence* (MIT Press, Cambridge, 1978).

[32] D. Lohse, Phys. Lett. A **196**, 70 (1994).

[33] G. I. Taylor, Proc. R. Soc. London, Ser. A **164**, 476 (1938).

[34] F. Chilla, S. Ciliberto, C. Innocenti, and E. Pampaloni, Europhys. Lett. **22**, 23 (1993).

[35] V. Yakhot, Phys. Rev. Lett. **63**, 1965 (1989).

[36] M. Rieutord and J.-P. Zahn, Astron. Astrophys. **296**, 127 (1995).

[37] A. Brandenburg, R. Jennings, A. Nordlund, M. Rieutord, R. Stein, and I. Tuominen, J. Fluid Mech. **306**, 325 (1996).